

*Reprinted from*

JAPANESE JOURNAL OF  
**APPLIED  
PHYSICS**

**REGULAR PAPER**

**Experimental Study of Silicon Monolayers for Future Extremely Thin  
Silicon-on-Insulator Devices: Phonon/Band Structures Modulation  
Due to Quantum Confinement Effects**

Tomohisa Mizuno, Keisuke Tobe, Yohichi Maruyama, and Toshiyuki Sameshima

Jpn. J. Appl. Phys. **51** (2012) 02BC03

# Experimental Study of Silicon Monolayers for Future Extremely Thin Silicon-on-Insulator Devices: Phonon/Band Structures Modulation Due to Quantum Confinement Effects

Tomohisa Mizuno\*, Keisuke Tobe, Yohichi Maruyama, and Toshiyuki Sameshima<sup>1</sup>

Kanagawa University, Hiratsuka, Kanagawa 259-1293, Japan

<sup>1</sup> Tokyo University of Agriculture and Technology, Koganei, Tokyo 184-8588, Japan

Received September 23, 2011; accepted November 29, 2011; published online February 20, 2012

We have experimentally studied Si monolayers, fabricated by thermal oxidation of silicon-on-insulator (SOI) substrates at high temperature, for future extremely thin SOI (ETSOI) complementary metal oxide semiconductor (CMOS) devices, and have shown the strong quantum confinement effects in the ETSOIs. We have successfully formed 0.52-nm Si monolayers, as confirmed by transmission electron microscopy (TEM) and a UV/visual reflection method. We have experimentally shown the asymmetric broadening and the peak downshift of the Raman peak of ETSOIs evaluated by UV-Raman spectroscopy, which is enhanced in the ETSOI thickness  $T_{\text{SOI}}$  of less than about 5 nm. These results are due to the quantum phonon confinement effects in ETSOIs. Using the TEM observation and UV-Raman spectroscopy of ETSOIs, we have also shown the tensile strain of ETSOIs due to the Si bending and the  $T_{\text{SOI}}$  variations in ETSOI substrates. In addition, we have observed photoluminescence (PL) from the ETSOIs with a  $T_{\text{SOI}}$  of less than about 5 nm and the PL intensity strongly depends on the  $T_{\text{SOI}}$ . However, the peak photon energy of about 1.85 eV in the PL spectrum is independent of the  $T_{\text{SOI}}$ . We cannot explain the PL results perfectly at present, but we have introduced a possible three-region model of electron/hole pair generation in a two-dimensional Si layer and electron/hole pair recombination at the Si/SiO<sub>2</sub> interface state region. © 2012 The Japan Society of Applied Physics

## 1. Introduction

Extremely thin silicon-on-insulator (ETSOI) metal oxide semiconductor field-effect transistors (MOSFETs) are candidates for future complementary MOS (CMOS) devices, because ETSOIs with an intrinsic Si channel can suppress both the short channel effects (SCEs) and the Coulomb scattering of the carriers in the channel.<sup>1,2)</sup> To suppress the SCEs of ETSOIs, the SOI thickness  $T_{\text{SOI}}$  should continue to decrease with scaling down of the effective channel length  $L_{\text{EFF}}$  of ETSOIs.

The quantum confinement effects (QCEs) in a thinner  $T_{\text{SOI}}$  structure cause the electron mobility modulation,<sup>3,4)</sup> which is due to the QCEs of electrons in ETSOIs, as well as the band gap  $E_G$  expansion of ETSOIs.<sup>5,6)</sup> In addition, the quantum phonon confinement (QPC) is enhanced in one-dimensional (1D) silicon (Si) semiconductors, such as Si nanowires and nanocrystals,<sup>7,8)</sup> compared with those of ETSOIs, which is evaluated by Raman spectroscopy.<sup>9–11)</sup> Therefore, the QPC induces the carrier mobility reduction owing to the enlarged phonon scattering of carriers even in ETSOIs.<sup>12)</sup>

On the other hand, the QCEs is reported to modulate the ETSOI band structures, and thus, to change the Si crystals to a direct band gap material from an indirect band gap semiconductor.<sup>5,13,14)</sup> In addition, even in the Si material, photoluminescence (PL) has been observed in low-dimensional porous-Si (p-Si),<sup>15)</sup> polycrystalline Si (poly-Si),<sup>16)</sup> and even thin film Si,<sup>14,17,18)</sup> which is caused by a strong QCEs. In particular, it is also reported that the  $T_{\text{SOI}}$  dependence of the peak photon energy is caused by the direct energy transmission in the direct band gap thin-film Si material changed from the indirect band gap bulk Si material.<sup>14)</sup> However, no detailed study on the QCEs in a Si monolayer structure including a discussion on the physical limitation on  $T_{\text{SOI}}$  has been carried out yet.

In this work, we have experimentally studied Si monolayers fabricated by thermal oxidation of SOI layers.<sup>19)</sup> We have successfully formed Si monolayers with  $T_{\text{SOI}}$  of about

0.5 nm, which is evaluated by high-resolution transmission electron microscopy (HRTEM), scanning TEM (STEM) with high-angle annular dark field (HAADF) and scanning bright field (SBF), and UV/visual reflectivity spectroscopy methods. Using UV-Raman spectroscopy, we have shown the strain effects caused by the Si bending in the Si monolayer and the QPC evaluated by the Raman peak broadening and downshift in  $T_{\text{SOI}}$  of less than 2.3 nm. In addition, we can also observe the visible PL spectrum from the ETSOIs at room temperature, which indicates the  $E_G$  expanding and the electron hole pair recombination at the Si/SiO<sub>2</sub> interface states.

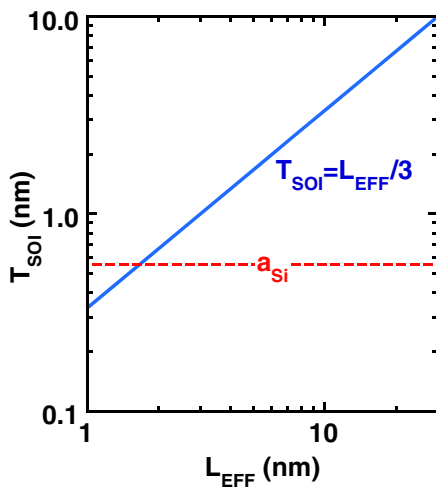
## 2. Experimental Procedure

Figure 1 shows the  $T_{\text{SOI}}$  design as a function of the  $L_{\text{EFF}}$  of ETSOIs to suppress the short channel effects, according to the empirical design law of  $T_{\text{SOI}} = L_{\text{EFF}}/3$ .<sup>1)</sup>  $T_{\text{SOI}}$  should continue to decrease with scaling down of  $L_{\text{EFF}}$ , and is equal to the lattice constant of Si,  $a_{\text{Si}}$  (0.54 nm), when  $L_{\text{EFF}} \approx 1.6$  nm. Therefore, it is very important for a future ETSOI-CMOS to study the Si monolayer, defined as the same  $T_{\text{SOI}}$  as having the  $a_{\text{Si}}$  in this study, and to clarify the physical properties of the Si monolayer.

To construct a well-controlled fabrication process for the ETSOIs and the Si monolayers, a (100) bonded SOI substrate<sup>20)</sup> can be thinned by a high-temperature O<sub>2</sub>/N<sub>2</sub> dry oxidation technique at 1100 °C for various oxidation times  $T_{\text{O}}$ , where the initial  $T_{\text{SOI}}$  is 55 nm and the buried oxide (BOX) thickness  $T_{\text{BOX}}$  is 150 nm. Under the oxidation conditions, a small oxidation even at the Si/BOX interface occurs, owing to internal thermal oxidation (ITOX) effects.<sup>21)</sup>

The  $T_{\text{SOI}}$  value is mainly evaluated by HRTEM, HAADF-STEM, and the UV/visual reflectivity spectrum. We have analyzed the physical properties of ETSOIs at room temperature by using UV-Raman spectroscopy and using a visible PL spectrum, where the He–Cd laser beam excitation wavelength is 325 nm (3.81 eV), the laser power is 1 mW, and the beam diameter is about 1 μm. In addition, since the laser penetration length  $\lambda_P$  in the Si layer is about 5 nm, it is possible to analyze the physical characteristics of ETSOIs.

\*E-mail address: mizuno@info.kanagawa-u.ac.jp



**Fig. 1.** (Color online) Scaling of  $T_{SOI}$  in ETSOIs to suppress the short channel effects of ETSOIs, using  $T_{SOI} = L_{EFF}/3$ .<sup>1)</sup>  $a_{Si}$  is the lattice constant of the Si semiconductor (0.54 nm).

### 3. Results and Discussion

#### 3.1 Si monolayer fabrication

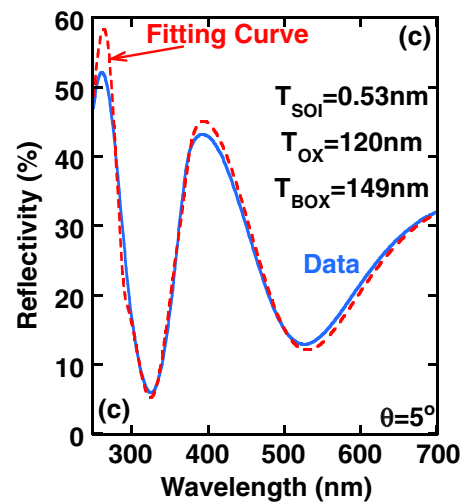
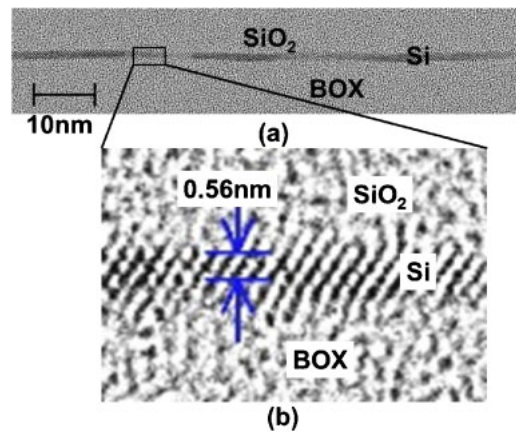
Figures 2(a) and 2(b) show the TEM and HRTEM images of the [110] cross section of the (100) Si monolayer, respectively. The  $T_{SOI}$  value of 0.56 nm is evaluated using the HRTEM image. Figure 2(c) also shows the UV/visual reflectivity spectrum of the Si monolayer, and the fitting curve indicates that the  $T_{SOI}$  value is about 0.53 nm, the surface thermal oxidation thickness  $T_{OX}$  is 120 nm, and the  $T_{BOX}$  is 149 nm. Therefore, the  $T_{SOI}$  value obtained by the HRTEM observation is the same as the  $T_{SOI}$  evaluated by the UV/visual reflection method. The  $T_{SOI}$  value is also consistent with the  $T_{SOI}$  value of 0.52 nm determined by using the HAADF-STEM image shown in Fig. 3. However, we have observed  $T_{SOI}$  variations and little Si bending in ETSOIs, as shown in Fig. 2(a).

Figure 3(a) shows clear Si atom images of the Si monolayer evaluated by the HAADF-STEM image, and indicates that the experimental dimensions of the Si monolayers are almost the same as those of the simulated image shown in Fig. 3(b) and both have a Si lattice constant of 0.54 nm.<sup>22)</sup> Considering the above  $T_{SOI}$  value of about 0.52 nm shown in Figs. 2 and 3, it is concluded that we have successfully formed a Si monolayer with the  $T_{SOI}$  of 0.52 nm using the thermal oxidation process of thin film SOI substrates.

The SBF-STEM image of the Si monolayer is shown in Fig. 4(a), showing the clear lattice spots in the whole Si regions, and thus the amorphous Si (a-Si) layer was not observed in the Si monolayers. Moreover, Fig. 4(b) shows the uniform HAADF-STEM image of ETSOIs, and thus shows no SiO<sub>2</sub> region formed by oxidizing the Si material through the Si monolayers.

#### 3.2 Phonon confinement effects evaluated by Raman spectroscopy

To study the phonon properties in ETSOIs, we have carried out UV-Raman spectroscopy for the ETSOIs with various  $T_{SOI}$  values. Figures 5(a)–5(c) show the experimental data



**Fig. 2.** (Color online) (a) TEM and (b) HRTEM images of the [110] cross section of the (100) Si monolayers fabricated by a thermal oxidation process of SOI substrates. (c) UV/visual reflectivity spectrum at the beam incident angle of 5° for 0.52-nm Si monolayers, where the solid line and the dashed line show the experimental data and the fitting curve with  $T_{OX} = 120$  nm,  $T_{SOI} = 0.53$  nm, and  $T_{BOX} = 149$  nm, respectively. (a) shows small  $T_{SOI}$  variations and small Si bending.

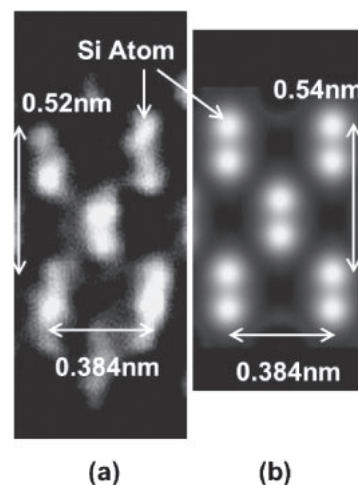


**Fig. 3.** (a) HAADF-STEM image for Si atoms and (b) simulated Si atom image of the [110] cross section of the Si monolayers. The white spots show the Si atoms, and the experimental  $a_{Si}$  (0.52 nm) in (a) is almost the same as the simulated results (0.54 nm) in (b).

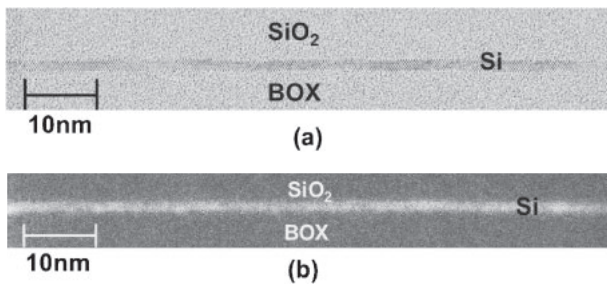


**Fig. 4.** (a) SBF-STEM image and (b) HAADF-STEM image of the [110] cross section of the Si monolayers at the same area. (a) and (b) show clear lattice spots and uniform Si crystal, respectively.

(solid lines) of UV-Raman spectroscopy under various  $T_{\text{SOI}}$  conditions. Since  $\lambda_P$  is 5 nm, we observe the Si Raman peak ( $520 \text{ cm}^{-1}$ ), even from the Si substrate under the BOX layer, when  $T_{\text{SOI}} < \lambda_P$ . The dashed lines show the net Raman peaks of the ETSOIs, for which the Si intensity  $I_{\text{Si}}$  of the Si substrates under the BOX is subtracted from the experimental intensity. Here,  $I_{\text{Si}}$  can be obtained by fitting the experimental Raman data at  $520 \text{ cm}^{-1}$  by Lorentzians/Gaussians and we have confirmed that the full width at half maximum (FWHM) of  $I_{\text{Si}}$  is almost the same as the FWHM of bulk Si. When  $T_{\text{SOI}}$  is thicker than 5.7 nm at least, Fig. 5(a) shows that the symmetric Raman peak of ETSOIs is the same peak as the normal Si ( $520 \text{ cm}^{-1}$ ), which originates from the usual threefold degenerate optical phonon mode. However, when  $0.52 \leq T_{\text{SOI}} \leq 2.3 \text{ nm}$ , Figs. 5(b) and 5(c) show the asymmetric broadening in a low frequency and the peak-downshift from  $520 \text{ cm}^{-1}$ . The asymmetric broadening and the downshift of the Raman shift are enhanced with decreasing  $T_{\text{SOI}}$ . As discussed in Fig. 4, it is clear that the Raman intensity below  $500 \text{ cm}^{-1}$  does not originate from the a-Si layer. Therefore, the asymmetric broadening of the net Raman shift of ETSOIs is attributable to the QPCs,<sup>7-11</sup> which relax both the momentum conservation and the selection rule in the Raman scattering, resulting in the various phonon modes of the Raman shift in two-dimensional (2D) ETSOIs. In addition, the Raman peak-downshift is due to both the QPC and the strain effects caused by the Si bending discussed in the next section.

The Raman spectrum of the Si nanowires and nanocrystals with a high heat resistance strongly depends on the laser power  $P_L$ .<sup>23</sup> Here, we discuss the  $P_L$  dependence of the Raman spectrum of ETSOIs. Figures 6(a) and 6(b) show the net Raman spectrum of the Si monolayers under various  $P_L$  conditions and the peak Raman shift from  $520 \text{ cm}^{-1}$ ,  $\Delta\omega$  vs  $P_L$ , respectively. As shown in Fig. 6(b), when  $P_L > 1 \text{ mW}$ ,  $\Delta\omega$  increases slightly, which is probably due to the self-heating of ETSOIs caused by  $P_L$ . However, when  $P_L \leq 1 \text{ mW}$ , the peak-downshift value and the FWHM value are almost independent of  $P_L$ . Therefore, the influence of  $P_L$  on the Raman spectrum of ETSOIs is considered to be small in our study, when  $P_L \leq 1 \text{ mW}$ .

Moreover, Fig. 7 shows the 2D mapping data for the Raman peak-downshift  $\Delta\omega$  of the Si monolayers from the Si peak ( $520 \text{ cm}^{-1}$ ) in a  $150 \mu\text{m}^2$  area.  $\Delta\omega$  varies widely, and the average and standard deviation are  $8.3$  and  $1.2 \text{ cm}^{-1}$ ,

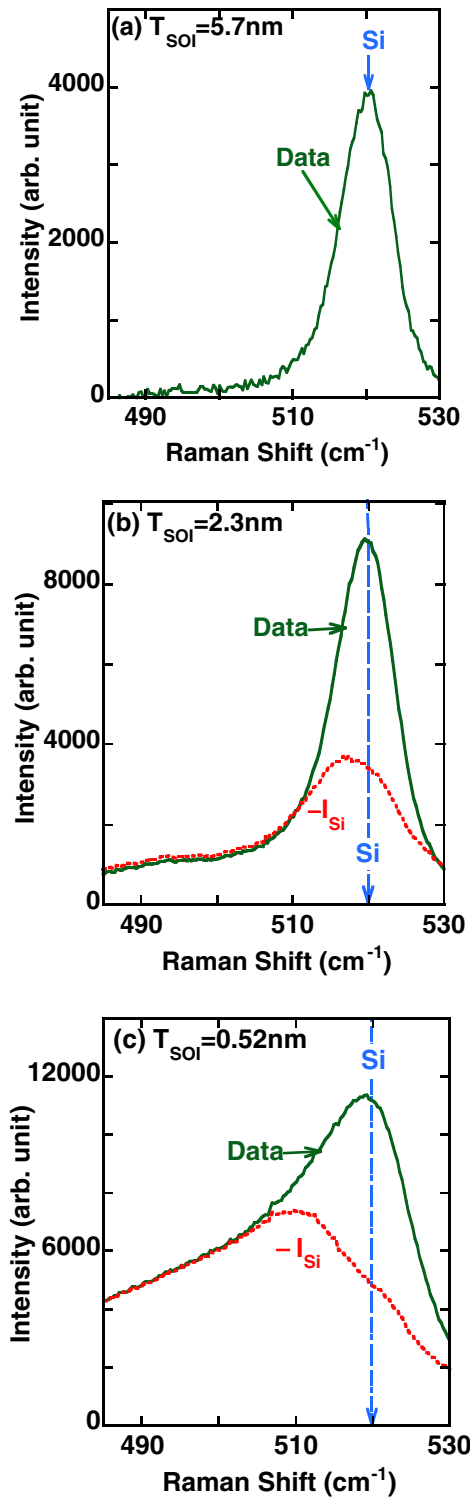


**Fig. 5.** (Color online) UV Raman spectra of ETSOIs with (a)  $T_{\text{SOI}} = 5.7 \text{ nm}$ , (b)  $T_{\text{SOI}} = 2.3 \text{ nm}$ , and (c)  $T_{\text{SOI}} = 0.52 \text{ nm}$ , where the He-Cd laser beam excitation wavelength is  $325 \text{ nm}$ , the laser power is  $1 \text{ mW}$ , the beam diameter is about  $1 \mu\text{m}$ , and the penetration length  $\lambda_P$  in the Si layer is about  $5 \text{ nm}$ . The  $520 \text{ cm}^{-1}$  Si peaks (arrows) in (b) and (c) originate from the Si substrate intensity  $I_{\text{Si}}$  under the BOX, because  $\lambda_P > T_{\text{SOI}}$ . The solid and dashed lines show the experimental data and the net intensity of the Si layers on the BOX, respectively. The net Raman data in (b) and (c) show the asymmetrical broadening and the peak-downshift.

respectively. The  $\Delta\omega$  variation is mainly caused by the variations of the  $T_{\text{SOI}}$ ,  $\Delta T_{\text{SOI}}$ , and the Si monolayer bending mentioned in Fig. 2(a), which will be discussed in the next section.

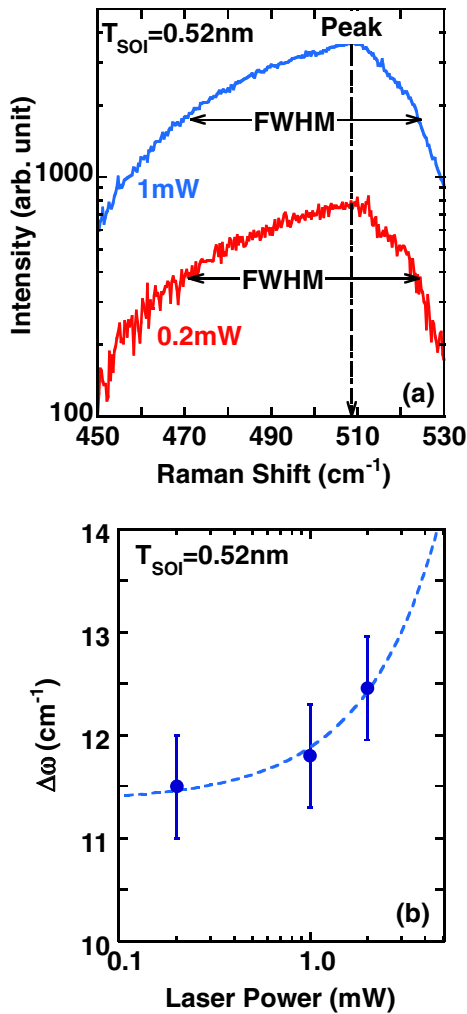


**Fig. 6.** (Color online) (a) Laser power dependence of the net Raman spectra of Si monolayers and (b)  $\Delta\omega$  as a function of laser power. The blue and red lines in (a) show the data of  $P_L$  of 1 and 0.2 mW, respectively. (b) indicates that the results can be fitted by an exponential function of laser power (dashed line). Error bars of  $\Delta\omega$  show the standard deviation of  $\Delta\omega$  obtained by the Raman spectroscopy measurement of 2D mapping ( $150\mu\text{m}^2$ ) of the Si monolayer.

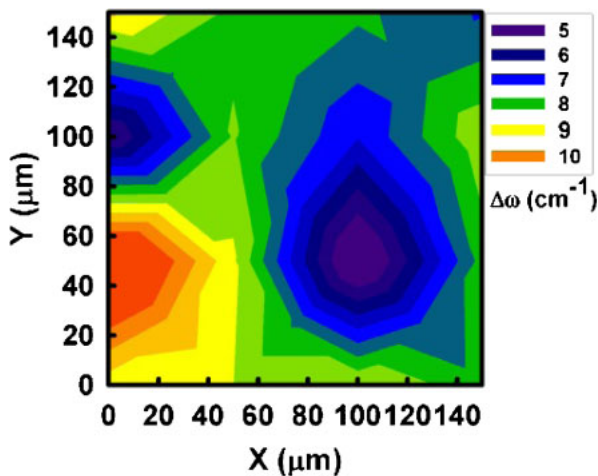


**Fig. 7.** (Color online) 2D mapping ( $150\mu\text{m}^2$ ) of Raman peak shift data  $\Delta\omega$  of Si monolayers from the Si peak of  $520\text{cm}^{-1}$ , where  $P_L$  is 1 mW. The average  $\Delta\omega$  and the standard deviation of  $\Delta\omega$  are  $8.3$  and  $1.2\text{cm}^{-1}$ , respectively.

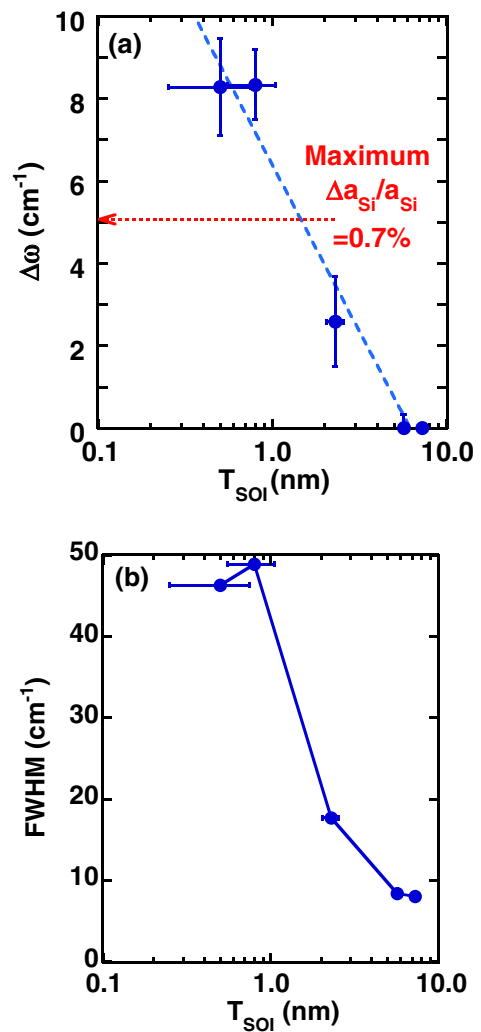


**Fig. 8.** (Color online)  $T_{\text{SOI}}$  dependence of (a)  $\Delta\omega$  and (b) FWHM value of the net Raman intensity, where  $P_L$  is 1 mW. The dotted arrow in (a) shows the calculated  $\Delta\omega$  due to the tensile strain value caused by the maximum Si monolayer bending shown in Fig. 9. The  $\Delta\omega$  and FWHM values rapidly increase when  $T_{\text{SOI}} < 5\text{ nm}$ . The dashed line of  $\Delta\omega \propto \ln T_{\text{SOI}}$  shows the fitting curve of the data in  $0.5 \leq T_{\text{SOI}} \leq 5.7\text{ nm}$ . Error bars of  $\Delta\omega$  and FWHM show the standard deviation of  $\Delta\omega$  and FWHM obtained by the Raman spectroscopy measurement of 2D mapping ( $150\mu\text{m}^2$ ) of the ETSOIs. In addition, the error bars of  $T_{\text{SOI}}$  of 0.25 nm is obtained by the standard deviation of  $\Delta\omega$ , using the relationship  $\Delta\omega \propto \ln T_{\text{SOI}}$ .

Figures 8(a) and 8(b) show the  $\Delta\omega$  and the FWHM values of the net Raman peaks of ETSOIs as a function of  $T_{\text{SOI}}$ , respectively. Both the  $\Delta\omega$  and FWHM suddenly increase at the critical  $T_{\text{SOI}}$  value of 2.3 nm and continue increasing with decreasing  $T_{\text{SOI}}$ , although the  $\Delta\omega$  and FWHM remain constant when the  $T_{\text{SOI}}$  is thicker than 5.7 nm. Therefore, the QPC and the tensile strain value in the ETSOI layers increase with decreasing  $T_{\text{SOI}}$ . The larger QPC effects in the ETSOIs are considered to enhance the phonon-scattering-induced mobility reduction of carriers.<sup>12)</sup> The QPC effect in the ETSOIs is the first physical limitation of the Si monolayer. Therefore, it is necessary to consider the QPC in designing the future ETSOI-CMOS. In addition, Fig. 8(a) indicates that the experimental data can be fitted by  $\Delta\omega \propto \ln T_{\text{SOI}}$ . Thus, the standard deviation of  $T_{\text{SOI}}$ ,  $\Delta T_{\text{SOI}}$ , of the Si monolayer in the  $150\mu\text{m}^2$  area is estimated to be about 0.25 nm, according to the  $\Delta\omega$  variation shown in the

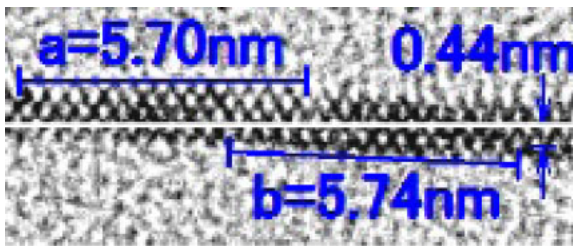


**Fig. 9.** (Color online) HRTEM image of the [110] cross section of the Si monolayer at the maximum Si bending area. The solid white line shows the horizontal Si/BOX interface at the flat Si monolayer region. As a result, the Si bending (arrows) was 0.44 nm. The horizontal length  $a$  of the lateral 15 Si atoms is 5.70 nm, resulting in the 0.38 nm space between each lateral Si atom. However, the slope length  $b$  of the lateral 15 Si atoms is 5.74 nm. As a result, the Si monolayers are tensilely strained and the strain value is about 0.7%.

map of the  $\Delta\omega$  of Fig. 7. The  $\Delta T_{\text{SOI}}$  value is almost the same as  $a_{\text{Si}}/2$ , which suggests that  $T_{\text{SOI}}$  variation is possibly caused by the surface roughness due to one Si atom layer step forming during the oxidation process of SOIs. The relatively large  $\Delta T_{\text{SOI}}$  is the first technical limitation of the Si monolayer in this study. However, the technical limitation of the  $\Delta T_{\text{SOI}}$  is possible to be suppressed by improving the fabrication process for the Si monolayers, such as the oxidation temperature.

### 3.3 Strain due to Si bending

In this section, we discuss the physical model for introducing the tensile strain into the ETSOIs.

We have already discussed the variations of the  $T_{\text{SOI}}$  and the Si monolayer bending in Fig. 2(a). Figure 9 shows the HRTEM image of the maximum Si bending area in the Si monolayer. The solid white line shows the horizontal Si/BOX interface in the flat Si monolayer region and thus, the maximum Si bending is 0.44 nm in this area. In addition, the horizontal length  $a$  of the lateral 15 Si atoms is 5.70 nm in the flat Si region. On the other hand, the slope length  $b$  of the lateral 15 Si atoms is 5.74 nm in the Si bending area. As a result, the Si monolayers in the bending region are tensilely strained, because of  $b > a$ , and the maximum strain value  $(b - a)/a$  is about 0.7%. Therefore, the  $\Delta\omega$  due to the maximum strain in this area corresponds to  $5.1 \text{ cm}^{-1}$ , according to the relationship of  $\Delta\omega \approx 725(b - a)/a$ .<sup>24,25)</sup> Moreover, another tensile strain, such as the thermal stress of the  $\text{SiO}_2$  on the Si monolayer, is considered to be smaller than that of the Si bending in this study. As a result, the maximum tensile strain due to the maximum Si bending can explain only 60% of the experimental  $\Delta\omega$  value ( $8.3 \text{ cm}^{-1}$ ) shown in Fig. 8(a). Thus, the  $\Delta\omega$  value is attributable to the peak-downshift due to the QPC as well as the tensile strain due to the Si bending. Moreover, the  $T_{\text{SOI}}$  dependence of the  $\Delta\omega$ , shown in Fig. 8(a), indicates that the Si bending increases with decreasing  $T_{\text{SOI}}$ , which is considered to be due to the surface thermal oxide layer stress to the Si layers on the BOX during the thermal oxidation process for ETSOIs. However, the influence of the local strain at the Si/SiO<sub>2</sub> interface<sup>26)</sup> on our Raman peak shift is not clear at present, and thus a further evaluation technique is necessary to measure the strain at the Si/SiO<sub>2</sub> interface other than

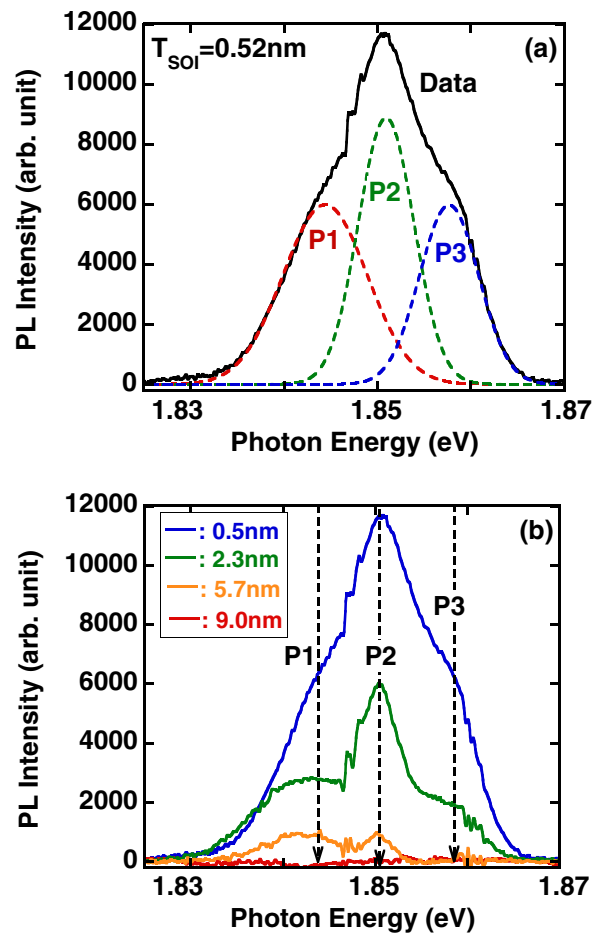


**Fig. 10.** (Color online) (a) PL spectrum (solid line) at  $T_{\text{SOI}} = 0.52 \text{ nm}$  and (b) PL spectrum at room temperature vs photon energy under various  $T_{\text{SOI}}$  conditions. The PL intensity is not observed in the  $T_{\text{SOI}}$  of more than 9 nm, and rapidly increases with decreasing  $T_{\text{SOI}}$  when the  $T_{\text{SOI}}$  is thinner than about 5 nm. (a) shows that the PL data can be fitted by three Gaussian curves (dashed lines) of P1 (1.843 eV at PL peak), P2 (1.850 eV at PL peak), and P3 (1.857 eV at PL peak). The dashed lines in (b) show P1, P2, and P3 peak energies and we cannot observe the P3 peak in the case of  $T_{\text{SOI}} = 5.7 \text{ nm}$ .

the Raman shift due to both QPC and the Si-bending. Consequently, the Si bending is the second technical limitation of the Si monolayer formation in this study, which is considered to be suppressed by improving the fabrication process for the ETSOIs.

### 3.4 Photoluminescence of ETSOIs

In this section, we discuss the PL results of ETSOIs. We can observe the PL intensity of a Si monolayer using the 3.81 eV excitation laser, since the  $\lambda_{\text{P}}$  in the Si layer is very small (5 nm).

As shown in Fig. 10(a), we can observe the room temperature PL spectrum vs photon energy  $h\nu$  ( $h$  is Planck constant and  $\nu$  is photon frequency) at the  $T_{\text{SOI}}$  of 0.52 nm, and the PL intensity can be fitted by the three Gaussian curves with different energy peaks of P1 (1.843 eV), P2 (1.850 eV), and P3 (1.857 eV). The physical mechanism for the different energy peaks is discussed later. However, in Fig. 10(b) shown as the PL spectrum of ETSOIs at room temperature vs photon energy under various  $T_{\text{SOI}}$  conditions, the PL intensities strongly depend on the  $T_{\text{SOI}}$  and rapidly

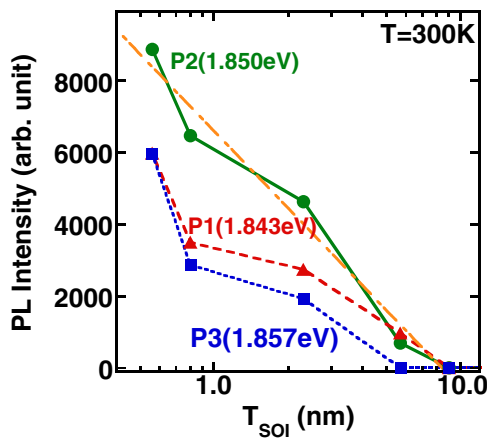


**Fig. 11.** (Color online) PL intensities of P1, P2, and P3 vs  $T_{\text{SOI}}$ . The PL intensities rapidly increase with decreasing  $T_{\text{SOI}}$ . We can observe the PL intensities of P1 and P2 at  $T_{\text{SOI}} \leq 5.7$  nm, but no PL intensity of P3 at  $T_{\text{SOI}} = 5.7$  nm. The dotted and dashed line show the fitting curve of P2 intensity, which is proportional to  $\ln T_{\text{SOI}}$ .

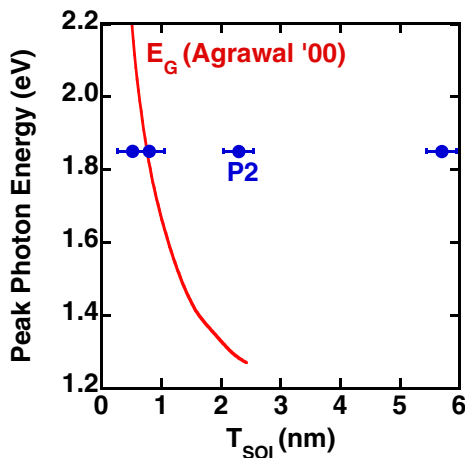


**Fig. 12.** (Color online) Peak photon energy of P2 vs  $T_{\text{SOI}}$ , where the solid line shows the theoretical  $E_G$  results reported by Agrawal *et al.*<sup>5)</sup> The circle shows the experimental peak photon energy of the ETSOIs in Fig. 10(a) and is completely independent of  $T_{\text{SOI}}$ . Both the P1 and P3 peak photon energies are also independent of  $T_{\text{SOI}}$ .

increase with decreasing  $T_{\text{SOI}}$ , when  $T_{\text{SOI}}$  is less than several nm. In addition, we cannot detect the PL intensity from the Si layers with the  $T_{\text{SOI}}$  of more than 9 nm. In the case of the  $T_{\text{SOI}}$  of 5.7 nm, we cannot observe the highest energy P3 peak, although we can detect both lower energy P1 and P2. Furthermore, in the range of  $1 < \text{photon-energy} < 3.6$  eV, we cannot detect the PL intensity from ETSOIs except at around 1.85 eV and thus, we cannot obtain the  $T_{\text{SOI}}$  dependence of the PL peak energy.

Here, Fig. 11 shows the  $T_{\text{SOI}}$  dependence of PL intensity of P1, P2, and P3 at room temperature. The P2 intensity is larger than the P1 and P3 intensities, but all P1, P2, and P3 intensities drastically increase with decreasing  $T_{\text{SOI}}$ . The laser photon flux absorption  $I_A$  in the Si layer with  $T_{\text{SOI}}$  is given by  $I_0 \cdot (1 - R) \cdot [1 - \exp(-a \cdot T_{\text{SOI}})]$ ,<sup>22)</sup> where  $I_0$  is the photon flux at the Si surface,  $R$  is the reflectivity at the Si surface, and  $a$  is the absorption coefficient of the photon (325 nm) in the Si layer and is about  $1/5 \text{ nm}^{-1}$  in this study.

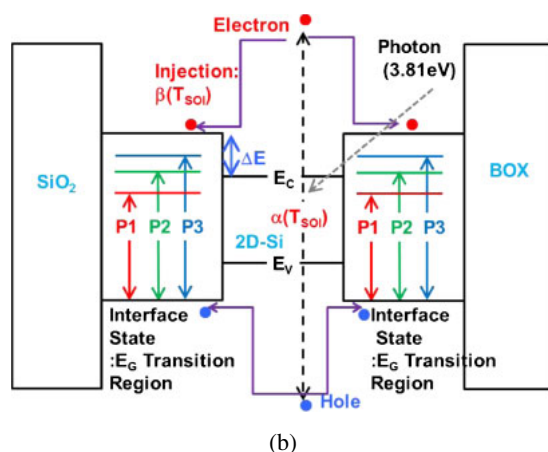
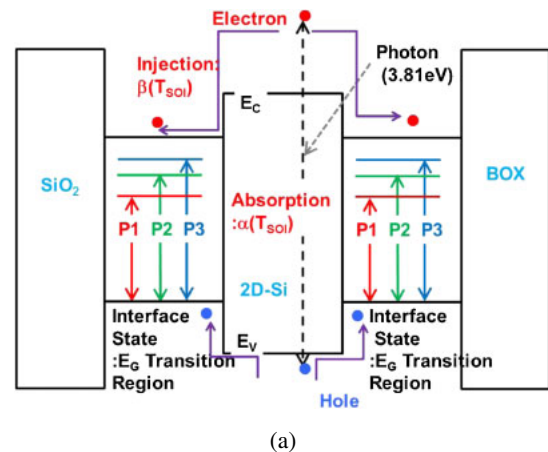


**Fig. 13.** (Color online) Three-region model of schematic band diagram for PL of ETSOIs (2D-Si) with electron/hole pair generation region in a 2D-Si layer and electron/hole pair recombination region in an  $E_G$  transition region of the Si/SiO<sub>2</sub> interface with three different energy levels.

(a)  $E_G > E_{G1}$  at  $T_{\text{SOI}} < 1$  nm, and (b)  $E_G < E_{G1}$  at  $1 \leq T_{\text{SOI}} < 5.7$  nm, where  $E_{G1}$  is the band gap of the Si/SiO<sub>2</sub> interface and  $E_{G1} > 1.86$  eV.  $\alpha(T_{\text{SOI}})$  and  $\beta(T_{\text{SOI}})$  are the photon flux absorption in 2D-Si and the injection rate of electron/hole pairs to the Si/SiO<sub>2</sub> interface, respectively.  $\Delta E$  shows the energy gap between the 2D-Si and the Si/SiO<sub>2</sub> interface. When photons (3.81 eV) are absorbed in 2D-Si, electron/hole pairs are generated in the 2D-Si, and are injected into the Si/SiO<sub>2</sub> interface regions. Injected electron/hole pairs are recombined, resulting in the photon emission at the Si/SiO<sub>2</sub> interface regions. The different peak photon energies with P1, P2, and P3 are due to the different interface energy states of P1, P2, and P3 in the Si/SiO<sub>2</sub> interface regions.

As a result, it is estimated that the  $I_A$  rapidly decreases with decreasing  $T_{\text{SOI}}$  and the  $I_A$  value at  $T_{\text{SOI}} = 0.52$  nm is about  $1/7$  of the  $I_A$  value at  $T_{\text{SOI}} = 5.7$  nm, if  $a$  and  $R$  are independent of  $T_{\text{SOI}}$ . The estimation results are opposite to the  $T_{\text{SOI}}$  dependence of the PL intensity in Fig. 11, which suggests that  $a$  increases with decreasing  $T_{\text{SOI}}$ , because of the modulated band structures of ETSOIs with  $T_{\text{SOI}}$  of less than several nm, as discussed later in Fig. 13.

On the other hand, Fig. 12 shows the experimental results of the peak photon energy of P2 and the theoretical band gap energy  $E_G$  of Si (solid line)<sup>5)</sup> as a function of  $T_{\text{SOI}}$ . P2 is completely independent of  $T_{\text{SOI}}$ , and is almost the same as the theoretical values only at a  $T_{\text{SOI}}$  of around 1 nm, while the QCEs theory (solid line) in ETSOIs shows that the  $E_G$  drastically increases with decreasing  $T_{\text{SOI}}$ . In addition, it is noted that P1 and P3 are also independent of  $T_{\text{SOI}}$ , which is

similar to the results reported by Takahashi *et al.*<sup>17)</sup> Therefore, the PL of ETSOIs in this study is not caused by the direct energy transmission in ETSOI layers with a direct band gap structure.

At present, we cannot explain the above PL phenomena of ETSOIs perfectly. Here, we introduce a possible simple model for the PL of ETSOIs, using a three-region model in which electron/hole pairs are generated in a 2D Si layer excited by high-energy laser photons and the electron/hole pair recombination occurs at the Si/SiO<sub>2</sub> interface state regions.<sup>17,18)</sup> Figure 13 shows a schematic band diagram of the 2D Si layer, the surface and the buried oxide layers, and the Si/SiO<sub>2</sub> interface state region, assuming that the surface interface characteristics are the same as those of the BOX interface. Since the Si/SiO<sub>2</sub> interface is not an entirely abrupt interface, the band gap of the Si/SiO<sub>2</sub> interface state regions  $E_{GI}$  gradually increases from the Si layer to the SiO<sub>2</sub> layer.<sup>27)</sup> Therefore, it is possible that  $E_{GI}$  becomes higher than 1.86 eV (highest P3 peak energy), as shown in Fig. 12, which indicates the  $E_G$  transition region in Fig. 13. Moreover, different energy state levels with P1, P2, and P3 exist in the Si/SiO<sub>2</sub> interface regions, and thus, the energy state levels are independent of  $T_{SOI}$ . However, the physical origin for the three energy state levels is not clear at present. It is expected that  $E_G$  of the 2D-Si layers is expanded by the QCEs of the 2D Si layer.<sup>5,6)</sup> Figures 13(a) and 13(b) show the case of  $E_G > E_{GI}$  at  $T_{SOI} < 1$  nm and the condition of  $E_G < E_{GI}$  at  $1 \leq T_{SOI} < 5.7$  nm, respectively, and  $E_G$  rapidly increases with decreasing  $T_{SOI}$ , as shown by the solid line in Fig. 12.  $\Delta E$  in Fig. 13(b) is the energy gap between the 2D-Si and the  $E_G$  transition regions, and  $\Delta E = (E_{GI} - E_G)/2$  and thus  $\Delta E$  depends on  $T_{SOI}$ . The electron/hole pairs are generated by the high-energy Laser photons (3.81 eV) in the 2D Si layer with the photon flux absorption  $\alpha(T_{SOI})$ . It is possible that  $\alpha(T_{SOI})$  increases with decreasing  $T_{SOI}$ , because the photon absorption coefficient is considered to increase with decreasing  $T_{SOI}$ , as discussed in Fig. 11. The generated electron/hole pairs are injected with the injection efficiency  $\beta(T_{SOI})$  into both Si/SiO<sub>2</sub> interface regions. Here,  $\beta(T_{SOI})$  can be given by  $\exp(-\Delta E/E_E)$ , where  $E_E$  is the generated electron energy and  $E_E = h\nu - E_G - E_{PN}$  ( $E_{PN}$  is phonon energy). In the case of an ultra thin Si layer, the photon direct transition in the 2D-Si can be assumed,<sup>14)</sup> resulting in  $E_{PN} = 0$ . When  $T_{SOI}$  increases,  $E_E$  increases with decreasing  $E_G$ , and  $\Delta E$  increases with decreasing  $E_G$ . Therefore, in the case of Fig. 13(b), since  $\beta(T_{SOI})$  weakly depends on  $T_{SOI}$ , the  $\beta(T_{SOI})$  reduction rate is only several tens of % at a thicker  $T_{SOI}$ , compared with  $\beta(T_{SOI})$  at  $\Delta E = 0$ . As a result, even at  $E_G < E_{GI}$  at  $1 < T_{SOI} < 5.7$  nm in Fig. 13(b), the generated electron/hole pairs can be injected into the Si/SiO<sub>2</sub> interface regions. On the other hand, photon emission occurs by the recombination of electron/hole pairs at the both the surface and the backside Si/SiO<sub>2</sub> interface regions. As a result, the PL peak photon energies, P1, P2, and P3 are determined by the energy state level in the Si/SiO<sub>2</sub> interface regions, and thus the PL peak photon energies are independent of  $T_{SOI}$ , as shown in Figs. 10 and 12. According to the weak  $T_{SOI}$  dependence of  $\beta(T_{SOI})$ , the rapid increase in the PL intensity in a thinner  $T_{SOI}$  shown in Fig. 11 is probably due to a rapid increase of  $\alpha(T_{SOI})$  in the thinner  $T_{SOI}$ . The above PL data

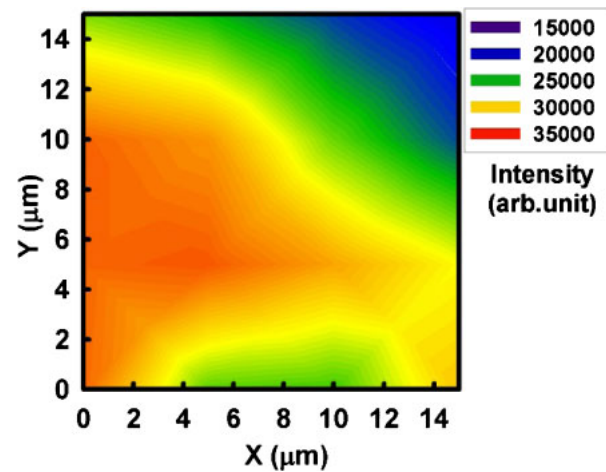


Fig. 14. (Color online) 2D mapping of PL intensity at the  $E_{PH}$  of 1.85 eV (P2) in a 15- $\mu\text{m}$  square area of the Si monolayer. The PL intensity fluctuates largely in the 15  $\mu\text{m}^2$  area.

are the indirect demonstration of the  $E_G$  expansion of ETSOIs in this study, and thus the  $E_G$  expansion of ETSOIs is the second physical limitation. On the other hand, when  $T_{SOI} > 9$  nm, the indirect phonon transition in the 2D-Si probably causes the rapid reduction of both  $\alpha(T_{SOI})$ <sup>22)</sup> and  $\beta(T_{SOI})$ . The rapid reduction of  $\beta(T_{SOI})$  is due to the  $E_E$  decrease in  $\beta(T_{SOI})$ , because  $E_{PN} \neq 0$ . As a result, we cannot observe the PL intensity of ETSOIs with a  $T_{SOI}$  thicker than 9 nm, as shown in Figs. 10 and 11. In addition, in the case of  $T_{SOI} = 5.7$  nm, since the  $\Delta E$  of the highest energy peak P3 is higher than the  $\Delta E$  of P1 and P2,  $\beta(T_{SOI})$  decreases, and thus the PL of P3 cannot be detected. Consequently, a further PL experiment, such as the excited photon energy dependence of the PL, is necessary to explain the PL results perfectly.

The  $E_G$  expansion is expected to suppress the leakage current of the source/drain pn junction in a future ETSOI, because the diffusion leakage current is proportional to  $\exp(-E_G/kT)$ ,<sup>28)</sup> and here,  $k$  is the Boltzmann constant and  $T$  is the lattice temperature. However, it is possible that the short channel effects of a future ETSOI-CMOS will be enhanced by the  $E_G$  increase, since the built-in potential  $V_{BI}$  is proportional to  $E_G$ <sup>28)</sup> and thus the depletion layer width of the source/drain pn junction is expanded by the  $E_G$  increase.

Next, Fig. 14 shows the 2D mapping of the PL intensity of the P2 peak (1.85 eV) shown in Fig. 10, and the PL intensity varies in a 15  $\mu\text{m}^2$  area. This is also due to the  $T_{SOI}$  variations, because the PL intensity strongly depends on  $T_{SOI}$  and the PL intensity is proportional to  $\ln T_{SOI}$ , as shown by the dotted/dashed line in Fig. 11. As a result, the  $T_{SOI}$  variation due to the PL intensity variation can be estimated to be about 0.3 nm, which is almost the same as the  $\Delta T_{SOI}$  value of 0.25 nm caused by  $\Delta\omega$  in Fig. 7. Therefore, the  $T_{SOI}$  variations, shown in Figs. 7 and 14, probably cause the fluctuations of both the QCEs and the electron confinement effect,<sup>3)</sup> resulting in larger mobility variation in future ETSOI-CMOS, as well as the  $E_G$  variations.

#### 4. Conclusions

We have experimentally studied Si monolayers for future ETSOI-CMOS fabricated by a thermal O<sub>2</sub>/N<sub>2</sub> dry oxidation

**Table I.** Physical/technical limitations of ETSOIs with  $T_{\text{SOI}}$  of less than several nm. The second column and the third column show the experimental results in this study and the expected device performances in a future ETSOI-CMOS, respectively. SCE and  $\mu$  indicate the short channel effects and the carrier mobility, respectively.

	Results	Device performance
Physical limitation	Phonon confinement	Mobility reduction
	$E_G$ expansion	Suppressed leak current, enhanced SCE
Technical limitation	$T_{\text{SOI}}$ variation	$\mu/E_G$ variation
	Si bending	Strain

process at high temperature and have shown the strong quantum confinement effects of the two-dimensional Si crystal. We have successfully formed the 0.52-nm Si monolayers confirmed by HRTEM, HAADF-STEM, and a UV/visual reflectivity spectrum method. Table I shows summary of the experimental results of a Si monolayer in this study. We have experimentally shown the asymmetric broadening and the peak downshift of the Raman peak of ETSOIs evaluated by UV-Raman spectroscopy, which is enhanced in the  $T_{\text{SOI}}$  of less than several nm. These results are due to the quantum phonon confinement in ETSOIs. The quantum phonon confinement in ETSOIs is considered to enhance the phonon-scattering-induced mobility reduction of carriers, which is the first physical limitation of the Si monolayer. Using UV-Raman spectroscopy, we have also shown the tensile strain of ETSOIs due to the Si bending and the  $T_{\text{SOI}}$  variations in ETSOI substrates, which are the technical limitations of the ETSOIs in this study. In addition, we have observed the photoluminescence (PL) from the ETSOIs with a  $T_{\text{SOI}}$  of less than about 5 nm and the PL intensity strongly depends on the  $T_{\text{SOI}}$ . However, the peak photon energy of about 1.85 eV is independent of the ETSOI thickness. We cannot explain the PL results perfectly at present, but we have introduced a possible three-region model in which an electron/hole pair is generated in a two-dimensional (2D) Si layer by high energy laser photons and the PL occurs at the Si/SiO<sub>2</sub> interface state region. The PL results suggest a modulation of band structures and the energy gap  $E_G$  expansion in the Si monolayers, which is expected to suppress the leak currents of the source/drain pn junctions in future ETSOIs. However, it is possible that the  $E_G$  expansion will induce the enhancement of the short channel effects of future ETSOIs. To overcome the technical limitations, it is necessary to improve the fabrication process for ETSOIs. Consequently, it is very important to consider

the quantum phonon confinement effects and the band modulation effects in 2D ETSOIs, in designing the future ETSOI-CMOS.

- 1) M. Yoshimi, M. Takahashi, S. Kambayashi, M. Kemmochi, H. Hazama, T. Wada, K. Kato, H. Tango, and K. Natori: *IEICE Trans. Electron.* **E74-C** (1991) 337.
- 2) A. Nazarov, J.-P. Colinge, F. Balestra, J.-P. Raskin, F. Gamiz, and V. S. Lysenko: *Semiconductor-on-Insulator Materials for Nanoelectronics Applications* (Springer, Berlin, 2011).
- 3) K. Uchida, H. Watanabe, A. Kinoshita, J. Koga, T. Numata, and S. Takagi: *IEDM Tech. Dig.*, 2002, p. 47.
- 4) G. Tsutsui, M. Saitoh, and T. Hiramoto: *IEEE Trans. Electron Devices* **26** (2005) 836.
- 5) B. K. Agrawal and S. Agrawal: *Appl. Phys. Lett.* **77** (2000) 3039.
- 6) Z. H. Lu and D. Grozea: *Appl. Phys. Lett.* **80** (2002) 255.
- 7) N. Fukata, T. Oshima, K. Murakami, T. Kizuka, T. Tsurui, and S. Ito: *J. Appl. Phys.* **100** (2006) 024311.
- 8) K. W. Adu, H. R. Gutierrez, and P. C. Eklund: in *Nanosilicon*, ed. V. Kumar (Elsevier, Amsterdam, 2008) Chap. 7.
- 9) H. Richter, Z. P. Wang, and L. Ley: *Solid State Commun.* **39** (1981) 625.
- 10) I. H. Campbell and P. M. Fauchet: *Solid State Commun.* **58** (1986) 739.
- 11) G. Faraci, S. Gibilisco, P. Russo, and A. R. Pennisi: *Phys. Rev. B* **73** (2006) 033307.
- 12) L. Donetti, F. Gámiz, J. B. Roldán, and A. Godoy: *J. Appl. Phys.* **100** (2006) 013701.
- 13) S. S. Iyer and Y.-H. Xie: *Science* **260** (1993) 40.
- 14) S. Saito, N. Sakuma, Y. Suwa, H. Arimoto, D. Hisamoto, H. Uchiyama, J. Yamamoto, T. Sakamizu, T. Mine, S. Kimura, T. Sugawara, M. Aoki, and T. Onai: *IEDM Tech. Dig.*, 2008, paper 19.5.
- 15) A. G. Cullis, L. T. Canham, and P. D. J. Calcott: *J. Appl. Phys.* **82** (1997) 909.
- 16) T. Sameshima, H. Watakabe, N. Andoh, and S. Higashi: *Jpn. J. Appl. Phys.* **45** (2006) 2437.
- 17) Y. Takahashi, T. Furuta, Y. Ono, T. Ishiyama, and M. Tabe: *Jpn. J. Appl. Phys.* **34** (1995) 950.
- 18) A. D. Lan, B. X. Liu, and X. D. Bai: *J. Appl. Phys.* **82** (1997) 5144.
- 19) T. Mizuno, K. Tobe, Y. Maruyama, and T. Sameshima: *Ext. Abstr. Solid State Devices and Materials*, 2011, p. 837.
- 20) <http://www.silvaco.com>
- 21) S. Nakashima, T. Katayama, Y. Miyamura, A. Matsuzaki, M. Kataoka, D. Ebi, M. Imai, K. Izumi, and N. Ohwada: *J. Electrochem. Soc.* **143** (1996) 244.
- 22) S. M. Sze and K. K. Ng: *Physics of Semiconductor Devices* (Wiley, New York, 2006).
- 23) S. Piscanec, M. Cantoro, A. C. Ferrari, J. A. Zapien, Y. Lifshitz, S. T. Lee, S. Hofmann, and J. Robertson: *Phys. Rev. B* **68** (2003) 241312(R).
- 24) G. Abstreiter, H. Brugger, T. Wolf, H. Jorke, and H. J. Herzog: *Phys. Rev. Lett.* **54** (1985) 2441.
- 25) T. Mizuno, N. Sugiyama, T. Tezuka, T. Numata, and S. Takagi: *IEEE Trans. Electron Devices* **50** (2003) 988.
- 26) H. Omi, T. Kawamura, S. Fujikawa, Y. Tsusaka, Y. Kagoshima, and J. Matsui: *Appl. Phys. Lett.* **86** (2005) 263112.
- 27) Y. Yamashita, S. Yamamoto, K. Mukai, J. Yoshinobu, Y. Harada, T. Tokushima, T. Takeuchi, Y. Takata, S. Shin, K. Akagi, and S. Tsuneyuki: *Phys. Rev. B* **73** (2006) 045336.
- 28) S. M. Sze: *Semiconductor Devices* (Wiley, New York, 2002).